Topological Temporal Boundary States in a Non-Hermitian Spatial Crystal

Ming-Wei Li,[1,2] Jian-Wei Liu,[1] Xulong Wang,[2] Wen-Jie Chen,[1,*] Guancong Ma,[2,†] and Jian-Wen Dong[1,‡]
[1]Department of Physics & State Key Laboratory of Optoelectronic Materials and Technologies, Sun Yat-sen University, Guangzhou 510275, China
[2]Department of Physics, Hong Kong Baptist University, Kowloon Tong, Hong Kong, China

(Received 11 February 2025; accepted 26 September 2025; published 27 October 2025)

Periodic modulation of the material index in time opens momentum gaps. Such systems are regarded as the temporal analog of common spatial crystals, wherein the band gaps open in frequency space. Recent studies have also led to the theoretical prediction of topological temporal boundary states (TTBSs) in such momentum gaps. In this Letter, we report the discovery and experimental realization of a new type of TTBS, appearing in a non-Hermitian spatial crystal with spatially periodic loss and gain, wherein the emergence of the Bloch momentum gap is associated with a parity-time broken phase, instead of relying on temporal modulation. By inducing a sudden flip of signs of the loss and gain profile, a mode emerges in the middle of the Bloch momentum gap and peaks at the flipping instant, which is regarded as a temporal boundary. Remarkably, we found that the temporal flip induces a topological transition in time, and the said mode is a TTBS that is a temporal analog of the Jackiw-Rebbi state. The TTBS is experimentally observed in a one-dimensional active mechanical lattice, and it can generically emerge in a wide range of non-Hermitian systems. By linking non-Hermitian physics with spatiotemporal topological systems, our results not only deepen the understanding of temporal topological phases but also open new grounds for controlling transient waves by topological means.

DOI: 10.1103/9b46-d2ry

Introduction—Time-varying media represent an emerging horizon for novel wave manipulation [1–14]. Periodic temporal modulation to material properties of a homogeneous material (e.g., the dielectric constant), can produce momentum band gaps [10,12,15–19], akin to energy gaps from periodic spatial potentials in common crystals [20,21]. In a momentum gap, modes grow or decay exponentially over time [16,17,19,22–25]. It has been theoretically shown in the context of a photonic time crystal (PTC) that the photonic momentum bands can exhibit distinct topology depending on the modulation profiles. A sudden change in the modulation profile creates a temporal boundary, driving the system from a topologically trivial to a nontrivial phase. Strikingly, this transition yields a topological temporal boundary state (TTBS) [26–31]. Although microwave PTC was experimentally realized recently [32], TTBS remains elusive due to challenges in achieving persistent temporal modulation with sufficient magnitude and rate [33].

Here, we discover that TTBS can be induced in a non-Hermitian spatial crystal (NSC) by a single temporal flip of its non-Hermiticity. By observing the temporal behaviors of growing and decaying modes in the *PT*-broken phase [34–47], we reveal that a Bloch momentum gap can be created by the spatial periodic modulation on the imaginary potential (i.e., gain or loss) without any temporal modulation, making them fundamentally distinct from those momentum gaps appearing in PTC, which are caused by temporal modulation to material index. A temporal sign flip in the gain-loss profile can trigger a topological phase transition in the Bloch momentum band structure. The TTBS, a temporal analog of a Jackiw-Rebbi state [48,49], appears and "localizes" at the transition instant. Unlike PTCs, the Bloch momentum gap in our system originates from the spatially periodic modulation of material properties, without resorting to temporal alternation of material properties. We experimentally observed the TTBS in a one-dimensional (1D) non-Hermitian mechanical lattice [50–54] and demonstrated its robustness against perturbation and disorder through simulations and experiments.

Topological state at the temporal boundary of a non-Hermitian spatial crystal—We begin with a 1D spatial crystal supporting classical waves governed by the Helmholtz equation:

$$\left[\frac{\mathrm{d}^2}{\mathrm{d}z^2}+\left(\frac{\omega}{c}\right)^2\rho(z)\right]\psi(z)=0, \tag{1}$$

where $\rho(z)=\{{}^{\rho_1=1-i\Gamma\quad [nd\le z<nd+d/2]}_{\rho_2=1+i\Gamma\,[nd+d/2\le z<(n+1)d]}$ is a system-dependent complex constitutive parameter including gain and loss, equivalent to a generalized squared refractive index. n is

*Contact author: chenwenj5@mail.sysu.edu.cn
†Contact author: phgcma@hkbu.edu.hk
‡Contact author: dongjwen@mail.sysu.edu.cn

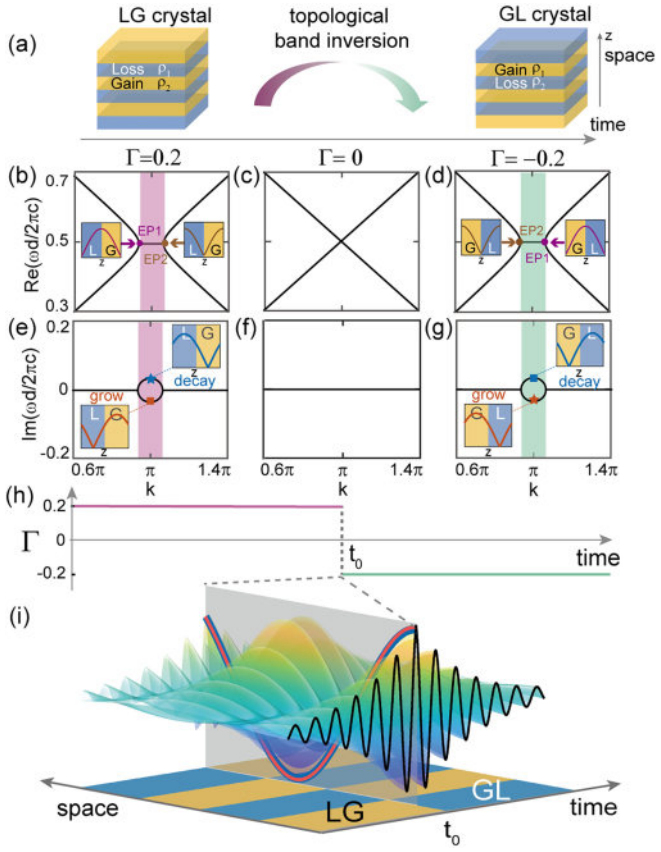

FIG. 1. TTBS between two NSCs. (a) Topological band inversion induced by non-Hermiticity Γ flipping in a 1D binary crystal. (b)–(g) Complex band structures for $\Gamma = 0.2, 0, -0.2$. As Γ flips sign, a topological band inversion occurs and two EPs swap their positions. (h) Temporal boundary occurs at time t_0. (i) Spatiotemporal profile of the TTBS localized at the temporal boundary: t_0; formed by the midgap grow mode in LG crystal ($t < t_0$) and the midgap decay mode in GL crystal ($t > t_0$). Red and blue lines: wave function at $t = t_0^-$ in LG crystal and at $t = t_0^+$ in GL crystal.

the number of unit cells, and c is the wave speed in a homogeneous medium. The imaginary part of $\rho(z)$ represents loss or gain, constituting the crystal's non-Hermiticity. The system can manifest as a photonic, acoustic, or mechanical crystal. Figure 1(a) shows two NSCs, loss-gain (LG) and gain-loss (GL) crystals, distinguished by their unit cell configurations. Band structures for three Γ values are shown in Figs. 1(b)–1(g), calculated via the transfer matrix method (see Supplemental Material [55]). When $\Gamma = 0$, the lattice reduces to a homogenous passive material with a linear dispersion [Figs. 1(c) and 1(f)]. When $\Gamma \neq 0$, these band structures open PT-broken regimes near $k = \pi$ [Figs. 1(b), 1(d), 1(e), and 1(g)]. Two complex bands with conjugate eigenfrequencies are found in this regime, which correspond to temporally growing or decaying bulk modes. Their temporal behaviors match those in a PTC momentum gap. These modes extract (dissipate) energy from (to) material gain (loss), rather than from (to) temporal modulation of refractive index [16,17,19,24] (see Supplemental Material [55]). Sections 4 and 5 of Ref. [55] prove that the PT-broken regime in NSC is indeed a Bloch momentum gap.

Figures 1(b)–1(g) show that the Bloch momentum gap closes and reopens as Γ changes sign. This loss-gain flip process swaps two band-edge states, i.e., EP1 (exceptional point 1) and EP2 modes [insets of Figs. 1(b) and 1(d)]. This flip is a topological transition, which will be proved later. Additionally, the eigenmode profiles in the LG (GL) crystals at $k = \pi$ [insets of Figs. 1(e) and 1(g)] reveal that the grow mode in LG and decay mode in GL share an identical spatial profile.

Now consider the following: initially, the grow mode in the LG crystal is excited. At time t_0, an instantaneous gain-loss flip (sign change in Γ) converts LG into GL. This flip acts as a temporal boundary [Fig. 1(h)], across which the lattice undergoes a topological transition. Figure 1(i) shows the spatiotemporal profile of the grow and decay modes across the boundary. The grow mode in LG completely couples to decay mode in GL (see Supplemental Material [55]), forming a TTBS peaked at t_0. It is spatially extended while temporally localized at t_0.

Topological characteristics of the NSCs—The topological characteristics of the NSCs is revealed by the parallel transport of its eigenmodes [62]. This transport is performed along a Bloch momentum band with ω as a parameter, thus the eigenmode is a function of ω instead of Bloch k, indicating that the Hamiltonian must be written with Bloch k as eigenvalues. To do so, we start from the static case of one NSC (LG or GL crystal) in Fig. 1(a). By solving Eq. (1), the eigenmode near the Brillouin zone boundary ($k = \pi$) approximately decomposes to $\psi(z) = A(\delta k)E_{+1} + B(\delta k)E_{-1}$ [63], where $\delta k = k - \pi$ is the deviation from $k = \pi$, $E_{+1} = e^{i(\delta k+\pi)z}$ and $E_{-1} = e^{i(\delta k-\pi)z}$ are the $+1$ and -1 Fourier components. $A(\delta k)$ and $B(\delta k)$ are the complex amplitudes of the two plane waves. We then obtain an effective Hamiltonian with $\delta\omega$ as eigenvalues

$$H_{\delta\omega}(\delta k) = \alpha(-im_\Gamma\sigma_y - c_3\delta k\sigma_z), \tag{2}$$

$$\text{with} \quad H_{\delta\omega}(\delta k)|\psi_{\delta\omega}(\delta k)\rangle = \delta\omega|\psi_{\delta\omega}(\delta k)\rangle, \tag{3}$$

and $m_\Gamma = \pi^2\sqrt{(\sqrt{\pi^2 + 4\Gamma^2} - \pi)/2\Gamma^2\pi^2}\Gamma$, $\delta\omega = \omega - \alpha c_0$. α, c_0, c_3 are constant coefficients. Equations (2) and (3) can be rewritten with δk as eigenvalue

$$H_{\delta k}(\delta\omega) = -\frac{1}{c_3}\left[\frac{\delta\omega}{\alpha}\sigma_z + m_\Gamma\sigma_x\right], \tag{4}$$

$$\text{with} \quad H_{\delta k}(\delta\omega)|\psi_{\delta k}(\delta\omega)\rangle = \delta k|\psi_{\delta k}(\delta\omega)\rangle. \tag{5}$$

The two eigenmomenta δk and the corresponding eigenvectors $|\psi_{\delta k}(\delta\omega)\rangle$ read

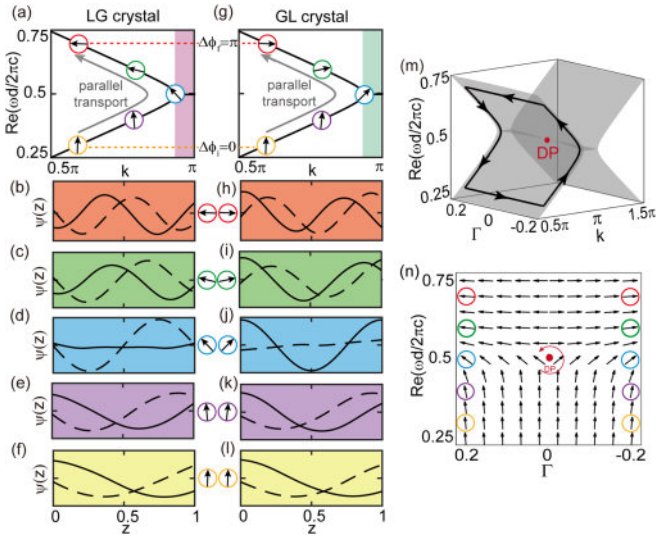

FIG. 2. Parallel transport of the eigenmodes along the momentum bands. (a),(g) Real band structures for LG and GL crystal on the left side of the gap. (b)–(f) Eigenmodes at five representative frequencies for LG crystal. Solid lines and dashed lines represent their real and imaginary part. (h)–(l) Eigenmodes for GL crystal. The gray arrows in (a) and (g) indicate the directions of parallel transport. The final states in (b) and (h) differ by a phase of π, indicating a topological transition. (m) A closed path defining Berry phase in ω-Γ synthetic space. (n) Eigenvectors with parallel transport gauge in the ω-Γ plane, with color circles corresponding to (b)–(f) and (h)–(l).

$$\delta k = \pm \frac{1}{c_3}\sqrt{m_\Gamma^2 + \left(\frac{\delta\omega}{\alpha}\right)^2}, \tag{6}$$

$$|\psi_{\delta k}(\delta\omega)\rangle = \frac{1}{N_2}\begin{bmatrix} m_\Gamma \\ -\frac{\delta\omega}{\alpha} \mp \sqrt{m_\Gamma^2 + \left(\frac{\delta\omega}{\alpha}\right)^2} \end{bmatrix}, \tag{7}$$

where N_2 is a normalized coefficient [55]. A PT-broken regime with $-|m_\Gamma|/c_3 < \delta k < |m_\Gamma|/c_3$ lies between the two EPs. Such momentum regime with complex conjugate frequencies can also appear in pseudo-Hermitian systems. They actually act as a Bloch momentum gap, which can be well interpreted using a simple two-band model [55].

Because of the absence of periodicity in ω, conventional closed-loop topological invariants are ill defined for the Bloch momentum band in our NSC. Instead, we use open-path parallel transports on Bloch momentum bands to characterize topology. We focus on the left side of the Bloch momentum band gap ($\delta k < 0$), shown in Figs. 2(a) and 2(g). Figures 2(b)–2(f) [2(h)–2(l)] plot eigenmodes at five representative frequencies in LG (GL) crystal. The middle columns depict two-component eigenvectors from the effective Hamiltonian. Equation (7) shows that the eigenvector at the low (high) frequency limit is always $[0,1]^{\mathrm{T}}$ ($[1,0]^{\mathrm{T}}$), regardless of m_Γ [55]. Notably, the eigenvectors are already nearly parallel to $[0,1]^{\mathrm{T}}$ ($[1,0]^{\mathrm{T}}$) at $0.3\times 2\pi c/d$ ($0.7\times 2\pi c/d$) in Figs. 2(f), 2(l) [2(b), 2(h)]. These are the start and finish points of the parallel transport. The same initial state, i.e., $[0,1]^{\mathrm{T}}$, is chosen for both the LG and GL crystals [Figs. 2(f) and 2(l)]. When parallelly transported along the respective Bloch band, two states rotate oppositely and evolve into two EP states at $0.4975\times 2\pi c/d$ [Figs. 2(d) and 2(j)], whose eigenvectors point upper left or upper right (blue circles). They both eventually evolve into $[1,0]^{\mathrm{T}}$ at the finish point, but their phases differ by π (red circles). This arises from two distinct EP modes, attributed to the band inversion.

For confirmation, we regard Γ as a synthetic dimension and extend the system to a 2D (Γ,ω) space where the Bloch bands close at $\Gamma = 0$ to form a linear crossing like a Dirac point [Fig. 2(m)]. Encircling the gap-closing point on the (Γ,ω) plane yields a Berry phase of π [Fig. 2(n)]. Thus, LG and GL crystals are 1D gapped topological phases obtained at opposite Γ, akin to gapping a Dirac point with opposite masses.

Temporal Jackiw-Rebbi state—It is counterintuitive that a Bloch momentum gap emerges in an NSC without temporal modulation. More interestingly, a topological transition of such an NSC would induce a protected TTBS. In fact, this TTBS is the temporal analog of a Jackiw-Rebbi state [49]. To illustrate, we consider the following dynamic equation based on the effective Hamiltonian in Eq. (2): $i(\partial/\partial t)|\psi(z,t)\rangle = \alpha(-im_\Gamma(t)\sigma_y - c_3\delta k\sigma_z)|\psi(z,t)\rangle$, where $m_\Gamma(t) = \pi^2\sqrt{(\sqrt{\pi^2+4\Gamma^2}-\pi)/2\Gamma^2\pi^2}\,\Gamma(t)$. In Fig. 1(h), $\Gamma(t) = 0.2\,\mathrm{step}(t-t_0) = \{^{0.2(t\le t_0)}_{-0.2(t>t_0)}$ is a step function indicating a sudden change in imaginary mass. Beyond the step function, the TTBS can exist for more general $\Gamma(t)$. In this case, the TTBS wave function has a Jackiw-Rebbi form [49]:

$$\psi(z,t) \propto \left(A(0)e^{i\pi z} + B(0)e^{-i\pi z}\right)e^{-i\alpha c_0 t}e^{\alpha\int^t dt' m_\Gamma(t')}. \tag{8}$$

It implies that the existence of the midgap TTBS only requires a sign change in temporal domain, i.e., $\Gamma(t\to-\infty) > 0$ and $\Gamma(t\to+\infty) < 0$. It does not rely on the specific form of $\Gamma(t)$, indicating strong robustness against temporal defect and disorder (see End Matter). However, TTBSs are sensitive to spatial defect and disorder. This is because spatial disorder prevents Bloch k from being a good quantum number, the midgap mode would be scattered to other momenta, causing the breakdown of the TTBS (see End Matter).

Observation of TTBS—Since our theory is based on a generic wave equation, TTBSs are not system specific and can emerge in various classical-wave systems. Here, we demonstrate TTBS with a mechanical lattice of spring-coupled active rotational oscillators [51,54] in a proof-of-principle experiment (see Supplemental Material [55]).

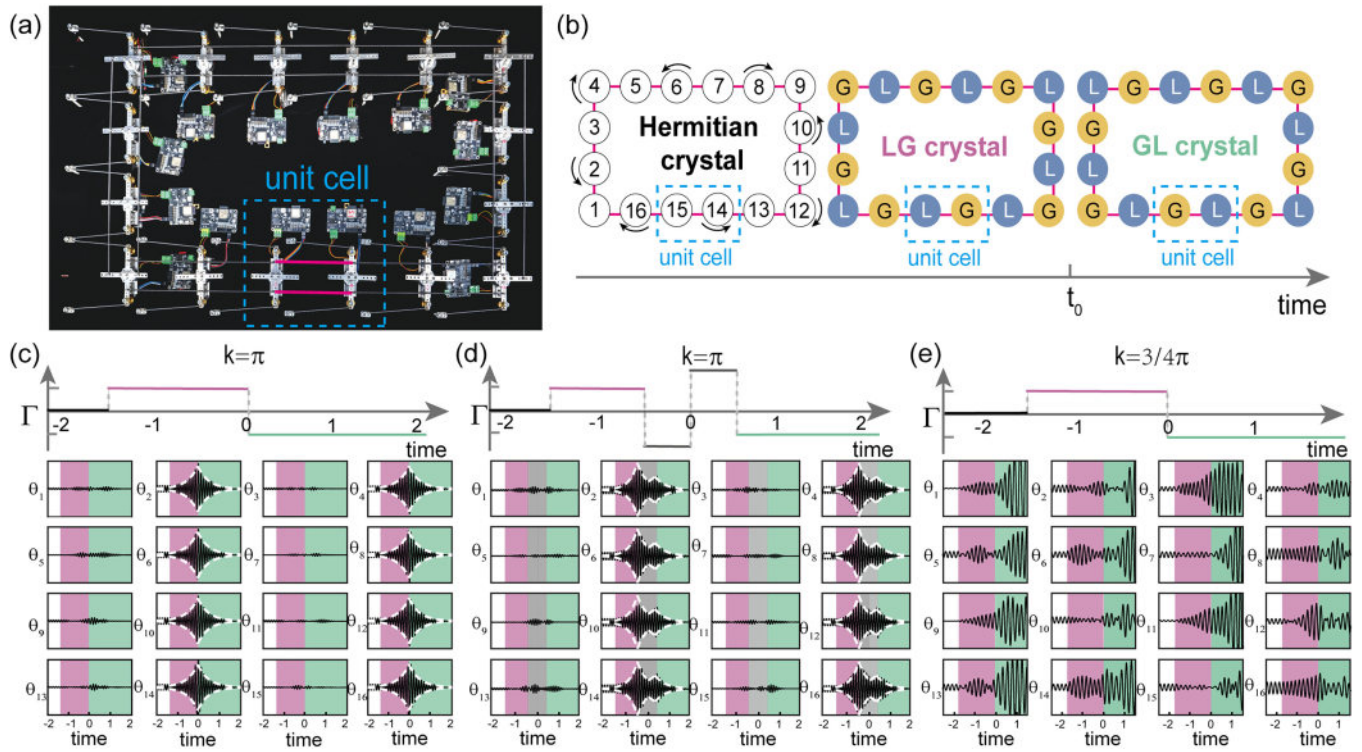

FIG. 3. Experimental observation of TTBS in 1D mechanical lattices. (a) Experimental setup of the active mechanical lattice. (b) Time modulation of the lattice. (c) Measured angular displacements of the TTBS between LG and GL crystals. The variation of non-Hermiticity $\Gamma(t)$ is plotted in the upper panel. The LG (GL) crystals are shaded in pink (green). (d) Measured angular displacements of the TTBS of a temporal boundary with disorder. (e) Measured angular displacements when the system is initially excited by a driving signal with $k = 3\pi/4$. TTBS peak is absent in this case.

A feedback control method is used to induce gain and loss. With low onsite resonant frequency of the oscillators, the electronic gain-loss flip occurs within milliseconds, much faster than the characteristic timescale of the grow-decay modes. Since TTBS is a spatial bulk state at $k = \pi$, we use two-site unit cells to form a closed 1D chain under Born–von Karman boundary condition. In this configuration, the lattice wave function $|\psi(x)\rangle = [\theta_1, \theta_2, ..., \theta_L]^T$ satisfies $\psi(x_j) = \psi(x_j + L)$, where θ_j is the measured angular displacement of the j th oscillator site and x_j is its position. The total number of sites is $L = 16$ in Fig. 3(a). Unlike traditional open-boundary lattices, this periodic condition ensures momentum quantization with Bloch $k = n\pi/4$. Active rotational oscillators achieve gain and loss via self-feedback torque $\tau_j(t) = \beta_j(t)\dot{\theta}_j(t)$, where $\dot{\theta}_j(t)$ is the instantaneous angular velocity of the j th oscillator. Here, $\beta_j(t)$, a step function flipping sign at $t_0 = 0$, determines the onsite gain-loss, corresponding to non-Hermiticity $\Gamma(t)$.The effect of $\tau_j(t)$ is gain or loss, depending on the sign of $\beta_j(t)$. The amplitude of $\beta_j(t)$ determines the gain-loss magnitude, which can be tuned by the controlling electronics.

To observe the TTBS, we first prepare the spatial mode at $k = \pi$ in a passive Hermitian lattice (without loss or gain, i.e., $\beta_j(t) = 0$). This mode is excited by driving the even-numbered oscillators with eight out-of-phase sinusoidal signals at $f = 8.1$ Hz [Fig. 3(b)]. This excitation profile matches the bipartite eigenmode at $k = \pi$ [55]. The lattice soon stabilizes into a steady bulk state [white background region in Fig. 3(c)]. Then, the active torques are switched on $[\beta_j(t) = 0 \to \beta_j(t) > 0]$, converting the system to the LG crystal configuration [Fig. 3(b)], and the oscillations of θ_j grow exponentially, indicating the grow mode [pink-shaded region in Fig. 3(c)]. After 1.3 s, $\beta_j(t)$ jumps, the system encounters the temporal boundary and flips to the GL crystal configuration $[\beta_j(t) > 0 \to \beta_j(t) < 0$, Fig. 3(b)]. The oscillations sharply turn from exponential growth to decay [Fig. 3(c)]. These observations confirm the existence of TTBS, and agree well with our theoretical prediction.

Discussions—We experimentally tested the robustness of TTBS with temporal disorder, as discussed in Fig. 4(e) (see End Matter), by inserting two temporal segments $(t \in [-0.5, 0.5])$ described by the $\Gamma(t)$ function in Fig. 3(d). The measured displacement fields for all 16 oscillators are plotted below. The TTBS is robust against disorder at the time boundary, but its profile is distorted.

The TTBS might appear to be an apparent phenomenon: a wave grows in a gain medium and then decays when the gain is replaced by loss. To clarify this, we compared by

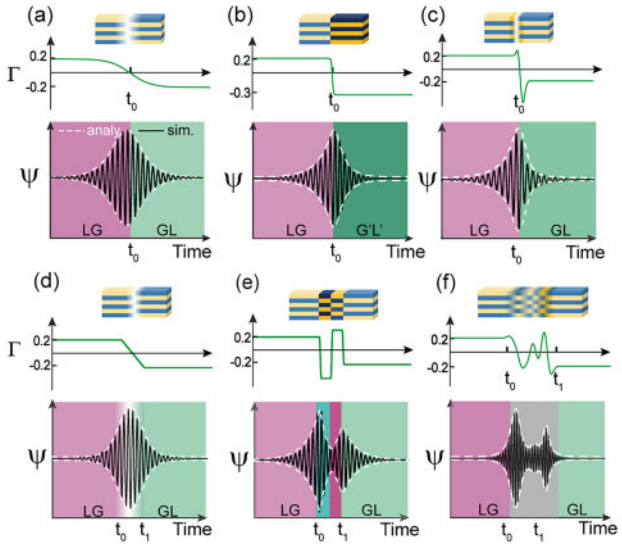

FIG. 4. Robustness of TTBS under temporal disorder. The upper panel shows six different temporal boundary profiles characterized by distinct forms of $\Gamma(t)$, including conventional temporal boundary: (a) a smooth boundary; (b) an asymmetric transition between an LG crystal and a G′L′ crystal ($\Gamma_{LG} = 0.2$, $\Gamma_{G'L'} = -0.3$); (c) an overshooting $\Gamma(t)$, and generalized boundary profiles: (d) a linearly ramped $\Gamma(t)$ boundary; (e) the two-segment boundary with different Γ values; and (f) a randomly fluctuated $\Gamma(t)$ profile. The corresponding wave evolutions in the lower panel confirm that TTBSs persist in all these cases, demonstrating their robustness across a broad range of temporal modulations.

exciting a spatial mode at $k = 3\pi/4$ within the Bloch momentum gap but it deviates from the midgap momentum [55]. We excited this mode by injecting 16 sinusoidal signals into different sites [Fig. 3(e)]. Unlike the midgap mode, the $k = 3\pi/4$ mode exhibited divergent behavior. The displacement field first grows in the LG crystal and continues growing even after flipping to GL crystal, where the gain is replaced by loss. The wave in the lattice oscillates and its amplitude eventually diverges. Notably, the temporal peak at t_0, which signifies the TTBS, is absent. These results agree well with our numerical simulation [55]. The deterioration of TTBS occurs gradually as the deviation of k increases. This is because when $\delta k \neq 0$ ($\delta k = k - \pi$), the grow mode in LG and the decay mode in GL are mismatched in their spatial profiles. Consequently, the grow-to-decay mode conversion is incomplete, leaving residual components that keep growing in GL crystal and eventually diverge. However, for small δk, the temporal localization persists to some extent (in a finite time). Therefore, the TTBS excitation is not restricted to a plane wave with $k = \pi$, a Gaussian wave packet with a finite k bandwidth can also generate it [55].

In summary, we discovered and observed a TTBS in an NSC through gain-loss flipping in time. The theoretical model relies only on a generic wave equation with spatially periodic PT-symmetric index, making it implementable across most classical wave systems [55]. Unlike TTBS in PTC, which requires persistent temporal modulation, our TTBS relies solely on spatial crystal and temporal non-Hermitian flipping. The gain-loss flipping is achievable via feedback control in active systems (such as our mechanical lattice) and with natural gain medium at a much faster timescale [55]. Our Letter extends the concept of topological phases for spatiotemporal scenarios and offers new routes for spatial and transient wave control. Even richer topological behaviors can be explored in 2D or 3D NSCs. The momentum selectivity suggests TTBS-based devices could enable novel functionalities in spectral filtering, beam shaping, and signal routing in integrated photonic systems [55].

Acknowledgments—M.-W. L. and G. M. thank Mathias Fink for discussion. This work was supported by the National Natural Science Foundation of China (62035016), National Key R&D Program of China (2022YFA1404400), Guangdong Basic and Applied Basic Research Foundation (2023B1515040023) and the Hong Kong Research Grants Council (RFS2223-2S01, 12301822), and the Hong Kong Baptist University (RC-RSRG/23-24/SCI/01, RC-SFCRG/23-24/R2/SCI/12).

Data availability—The data that support the findings of this article are not publicly available. The data are available from the authors upon reasonable request.

[1] B. A. Auld, J. H. Collins, and H. R. Zapp, Signal processing in a nonperiodically time-varying magnetoelastic medium, Proc. IEEE **56**, 258 (1968).
[2] L. Felsen and G. Whitman, Wave propagation in time-varying media, IEEE Trans. Antenna Propag. **18**, 242 (1970).
[3] J. T. Mendonca and P. K. Shukla, Time refraction and time reflection: Two basic concepts, Phys. Scr. **65**, 160 (2002).
[4] V. Bacot, M. Labousse, A. Eddi, M. Fink, and E. Fort, Time reversal and holography with spacetime transformations, Nat. Phys. **12**, 972 (2016).
[5] M. Camacho, B. Edwards, and N. Engheta, Achieving asymmetry and trapping in diffusion with spatiotemporal metamaterials, Nat. Commun. **11**, 3733 (2020).
[6] H. Li and A. Alù, Temporal switching to extend the bandwidth of thin absorbers, Optica **8**, 24 (2020).
[7] V. Pacheco-Peña and N. Engheta, Temporal aiming, Light Sci. Appl. **9**, 129 (2020).
[8] V. Pacheco-Peña and N. Engheta, Antireflection temporal coatings, Optica **7**, 323 (2020).
[9] H. Li, S. Yin, E. Galiffi, and A. Alù, Temporal parity-time symmetry for extreme energy transformations, Phys. Rev. Lett. **127**, 153903 (2021).
[10] E. Galiffi, R. Tirole, and S. Yin, Photonics of time-varying media, Adv. Opt. Photonics **4**, 014002 (2022).
[11] R. Tirole, E. Galiffi, J. Dranczewski, T. Attavar, B. Tilmann, Y.-T. Wang, P. A. Huidobro, A. Alù, J. B. Pendry, S. A. Maier, S. Vezzoli, and R. Sapienza, Saturable time-varying

mirror based on an epsilon-near-zero material, Phys. Rev. Appl. **18**, 054067 (2022).
[12] S. Yin, E. Galiffi, and A. Alù, Floquet metamaterials, eLight **2**, 8 (2022).
[13] S. Hidalgo-Caballero, S. Kottigegollahalli Sreenivas, V. Bacot, S. Wildeman, M. Harazi, X. Jia, A. Tourin, M. Fink, A. Cassinelli, M. Labousse, and E. Fort, Damping-driven time reversal for waves, Phys. Rev. Lett. **130**, 087201 (2023).
[14] H. Moussa, G. Xu, S. Yin, E. Galiffi, Y. Ra'di, and A. Alù, Observation of temporal reflection and broadband frequency translation at photonic time interfaces, Nat. Phys. **19**, 863 (2023).
[15] J. R. Reyes-Ayona and P. Halevi, Observation of genuine wave vector (k or β) gap in a dynamic transmission line and temporal photonic crystals, Appl. Phys. Lett. **107**, 074101 (2015).
[16] M. Lyubarov, Y. Lumer, A. Dikopoltsev, E. Lustig, Y. Sharabi, and M. Segev, Amplified emission and lasing in photonic time crystals, Science **377**, 425 (2022).
[17] Y. Sharabi, A. Dikopoltsev, E. Lustig, Y. Lumer, and M. Segev, Spatiotemporal photonic crystals, Optica **9**, 585 (2022).
[18] E. Lustig, O. Segal, S. Saha, C. Fruhling, V. M. Shalaev, A. Boltasseva, and M. Segev, Photonic time-crystals—Fundamental concepts, Opt. Express **31**, 9165 (2023).
[19] Y. Pan, M.-I. Cohen, and M. Segev, Superluminal k-gap solitons in nonlinear photonic time crystals, Phys. Rev. Lett. **130**, 233801 (2023).
[20] B. A. Bernevig, *Topological Insulators and Topological Superconductors* (Princeton University Press, Princeton, NJ, 2013).
[21] T. Ozawa, H. M. Price, A. Amo, N. Goldman, M. Hafezi, L. Lu, M. C. Rechtsman, D. Schuster, J. Simon, O. Zilberberg, and I. Carusotto, Topological photonics, Rev. Mod. Phys. **91**, 015006 (2019).
[22] C. Caloz and Z. L. Deck-Léger, Spacetime metamaterials—Part II: Theory and applications, IEEE Trans. Antenna Propag **68**, 1583 (2020).
[23] S. Lee, J. Park, H. Cho, Y. Wang, B. Kim, C. Daraio, and B. Min, Parametric oscillation of electromagnetic waves in momentum band gaps of a spatiotemporal crystal, Photonics Res. **9**, 142 (2021).
[24] Y. Sharabi, E. Lustig, and M. Segev, Disordered photonic time crystals, Phys. Rev. Lett. **126**, 163902 (2021).
[25] S. Sadhukhan and S. Ghosh, Bandgap engineering and amplification in photonic time crystals, J. Opt. **26**, 045601 (2024).
[26] E. Lustig, Y. Sharabi, and M. Segev, Topological aspects of photonic time crystals, Optica **5**, 1390 (2018).
[27] J. Ma and Z. G. Wang, Band structure and topological phase transition of photonic time crystals, Opt. Express **27**, 12914 (2019).
[28] R. Y. Dong, Y. M. Liu, J. Y. Sui, and H. F. Zhang, Band structure and temporal topological edge state of continuous photonic time crystals, IEEE Trans. Antenna Propag. **72**, 674 (2024).
[29] J. Feis, S. Weidemann, T. Sheppard, H. M. Price, and A. Szameit, Space-time-topological events in photonic quantum walks, Nat. Photonics **19**, 518 (2025).
[30] M. Lin, S. Ahmed, M. Jamil, Z. Liang, Q. Wang, and Z. Ouyang, Temporally-topological defect modes in photonic time crystals, Opt. Express **32**, 9820 (2024).
[31] W. Zhu and J.-H. Jiang, Characterizing generalized Floquet topological states in hybrid space-time dimensions, arXiv: 2409.09937.
[32] X. Wang, M. S. Mirmoosa, V. S. Asadchy, C. Rockstuhl, S. Fan, and S. A. Tretyakov, Metasurface-based realization of photonic time crystals, Sci. Adv. **9**, eadg7541 (2023).
[33] A. Boltasseva, V. M. Shalaev, and M. Segev, Photonic time crystals: from fundamental insights to novel applications: opinion, Opt. Mater. Express **14**, 592 (2024).
[34] C. M. Bender and S. Boettcher, Real spectra in non-Hermitian Hamiltonians having PT symmetry, Phys. Rev. Lett. **80**, 5243 (1998).
[35] A. Mostafazadeh, Pseudo-Hermiticity versus PT symmetry: The necessary condition for the reality of the spectrum of a non-Hermitian Hamiltonian, J. Math. Phys. (N.Y.) **43**, 205 (2002).
[36] C. M. Bender, Making sense of non-Hermitian Hamiltonians, Rep. Prog. Phys. **70**, 947 (2007).
[37] R. El-Ganainy, K. G. Makris, D. N. Christodoulides, and Z. H. Musslimani, Theory of coupled optical PT-symmetric structures, Opt. Lett. **32**, 2632 (2007).
[38] S. Klaiman, U. Günther, and N. Moiseyev, Visualization of branch points in PT-symmetric waveguides, Phys. Rev. Lett. **101**, 080402 (2008).
[39] K. G. Makris, R. El-Ganainy, D. N. Christodoulides, and Z. H. Musslimani, Beam dynamics in PT symmetric optical lattices, Phys. Rev. Lett. **100**, 103904 (2008).
[40] A. Guo, G. J. Salamo, D. Duchesne, R. Morandotti, M. Volatier-Ravat, V. Aimez, G. A. Siviloglou, and D. N. Christodoulides, Observation of PT-symmetry breaking in complex optical potentials, Phys. Rev. Lett. **103**, 093902 (2009).
[41] C. E. Rüter, K. G. Makris, R. El-Ganainy, D. N. Christodoulides, M. Segev, and D. Kip, Observation of parity-time symmetry in optics, Nat. Phys. **6**, 192 (2010).
[42] A. Regensburger, C. Bersch, M.-A. Miri, G. Onishchukov, D. N. Christodoulides, and U. Peschel, Parity-time synthetic photonic lattices, Nature (London) **488**, 167 (2012).
[43] L. Feng, R. El-Ganainy, and L. Ge, Non-Hermitian photonics based on parity-time symmetry, Nat. Photonics **11**, 752 (2017).
[44] R. El-Ganainy, K. G. Makris, M. Khajavikhan, Z. H. Musslimani, S. Rotter, and D. N. Christodoulides, Non-Hermitian physics and PT symmetry, Nat. Phys. **14**, 11 (2018).
[45] H. Zhao and L. Feng, Parity-time symmetric photonics, Natl. Sci. Rev. **5**, 183 (2018).
[46] S. K. Ozdemir, S. Rotter, F. Nori, and L. Yang, Parity-time symmetry and exceptional points in photonics, Nat. Mater. **18**, 783 (2019).
[47] S. K. Gupta, Y. Zou, X. Y. Zhu, M. H. Lu, L. J. Zhang, X. P. Liu, and Y. F. Chen, Parity-time symmetry in non-Hermitian complex optical media, Adv. Mater. **32**, e1903639 (2020).
[48] R. Jackiw and C. Rebbi, Solitons with fermion number 1/2, Phys. Rev. D **13**, 3398 (1976).

[49] S. Q. Shen, *Topological Insulators: Dirac Equation in Condensed Matter* (Springer Science & Business Media, New York, 2017).
[50] L. M. Nash, D. Kleckner, A. Read, V. Vitelli, A. M. Turner, and W. T. M. Irvine, Topological mechanics of gyroscopic metamaterials, Proc. Natl. Acad. Sci. U.S.A. **112**, 14495 (2015).
[51] W. Wang, X. Wang, and G. Ma, Non-Hermitian morphing of topological modes, Nature (London) **608**, 50 (2022).
[52] W. Wang, X. Wang, and G. Ma, Extended state in a localized continuum, Phys. Rev. Lett. **129**, 264301 (2022).
[53] X. Cui, R.-Y. Zhang, X. Wang, W. Wang, G. Ma, and C. T. Chan, Experimental realization of stable exceptional chains protected by non-Hermitian latent symmetries unique to mechanical systems, Phys. Rev. Lett. **131**, 237201 (2023).
[54] W. Wang, M. Hu, X. Wang, G. Ma, and K. Ding, Experimental realization of geometry-dependent skin effect in a reciprocal two-dimensional lattice, Phys. Rev. Lett. **131**, 207201 (2023).
[55] Supplemental Material at http://link.aps.org/supplemental/10.1103/9b46-d2ry of Topological Temporal Boundary States in a Non-Hermitian Spatial Crystal, which includes Refs. [56–61], for additional information about the derivations and the numerical simulations.
[56] W. P. Su, J. R. Schrieffer, and A. J. Heeger, Solitons in polyacetylene, Phys. Rev. Lett. **42**, 1698 (1979).
[57] A. Dutt, M. Minkov, I. A. D. Williamson, and S. Fan, Higher-order topological insulators in synthetic dimensions, Light Sci. Appl. **9**, 131 (2020).
[58] K. Ding, G. Ma, M. Xiao, Z. Q. Zhang, and C. T. Chan, Emergence, coalescence, and topological properties of multiple exceptional points and their experimental realization, Phys. Rev. X **6**, 021007 (2016).
[59] X. Zhu, C. Qian, E. Li, and H. Chen, Negative conductivity induced reconfigurable gain metasurfaces and their nonlinearity, Phys. Rev. Lett. **133**, 113801 (2024).
[60] X. Feng, T. Wu, Z. Gao, H. Zhao, S. Wu, Y. Zhang, L. Ge, and L. Feng, Non-Hermitian hybrid silicon photonic switching, Nat. Photonics **19**, 264 (2025).
[61] A. Regensburger, C. Bersch, M. A. Miri, G. Onishchukov, D. N. Christodoulides, and U. Peschel, Parity-time synthetic photonic lattices, Nature (London) **488**, 167 (2012).
[62] R. Raffaele, Manifestations of Berry's phase in molecules and condensed matter, J. Phys. Condens. Matter **12**, R107 (2000).
[63] K. Ding, Z. Q. Zhang, and C. T. Chan, Coalescence of exceptional points and phase diagrams for one-dimensional *PT*-symmetric photonic crystals, Phys. Rev. B **92**, 235310 (2015).

End Matter

Temporal robustness of the TTBS—Within the two-band approximation and under preserved *PT* symmetry ensuring a well-defined Bloch momentum gap, the TTBS can be regarded as a temporal analog of the Jackiw-Rebbi state. Its formation requires that the imaginary Dirac mass undergoes a sign change near the temporal boundary. As such, the existence of the TTBS does not rely on the specific form of $\Gamma(t)$, demonstrating strong robustness against temporal defects and disorders. For example, the TTBS persists when $\Gamma(t)$ changes sign smoothly instead of sharply, as shown in Fig. 4(a), where the resulting peak becomes broader but remains localized. It also survives overshoots in $\Gamma(t)$ before or after the flip [Fig. 4(b)], and even for an asymmetric profile near the boundary, e.g., $\Gamma_{LG} = 0.2$ and $\Gamma_{G'L'} = -0.3$ before and after the flip, respectively [Fig. 4(c)].

In these results, the temporal envelope of the TTBS can be shaped by choosing the form of $\Gamma(t)$. This property is readily implied in Eq. (8). This dependence provides a flexible route for transient wave control. To further explore this, we consider more boundary profiles: a linear ramp [Fig. 4(d)], multiple jumps [Fig. 4(e)]; and a randomly fluctuating profile [Fig. 4(f)]. In all cases, the TTBS remains clearly observable—even displaying "elongated" and "multipeaked" features under complex modulations—highlighting its resilience and potential utility in dynamic wave manipulation. Additionally, our schemes are applicable to any *PT*-symmetric or pseudo-Hermitian system, such as a ternary-quaternary crystal (see Supplemental Material [55]).

The TTBS is sensitive to spatial disorder—This is because the existence of the Bloch k gap fundamentally hinges on Bloch k being a good quantum number, i.e., it must conserve throughout the temporal process. Spatial disorder breaks the spatial periodicity, thereby rendering the Bloch k ill defined. To show the criticality associated with Bloch k, we calculate the evolution of the midgap mode across a temporal boundary between an LG crystal and a spatially disordered GL crystal

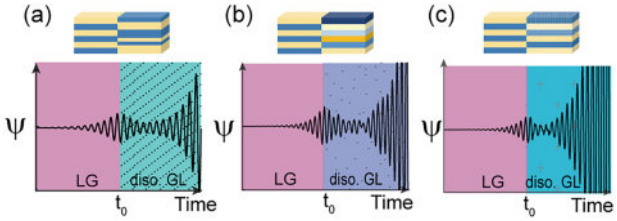

FIG. 5. TTBS is sensitive to spatial disorder. The upper panel illustrates three types of spatial disorder introduced into the GL crystal: (a) randomly perturbed layer thicknesses while maintaining the overall lattice period; (b) uniform thicknesses but randomly varied gain-loss strengths; (c) fixed geometry and non-Hermiticity, but random variations in the real part of ρ. In all three cases, the field diverges after entering the disordered GL crystal, indicating the breakdown of TTBS.

under three types of spatial disorder, as illustrated in the upper panel of Fig. 5: (a) random layer thicknesses: where $d_L = [0.5 + 0.05 \times \mathrm{rand}(-1, 1)]d$, with $d_G = d - d_L$; (b) uniform thicknesses but randomly varied gain-loss strengths: $\Gamma = -0.2 + 0.15 \times \mathrm{rand}(-1, 1)$; and (c) fixed geometry and Γ, but with random variations in the real part of ρ: $\mathrm{Re}(\rho_{L\backslash G}) = 1 + 0.6 \times \mathrm{rand}(-1, 1)$. In all three cases, the field diverges after the system enters the disordered GL crystal, indicating the breakdown of the TTBS.